Polarization dependence of the ac Stark effect in multiphoton transitions of diatomic molecules

Bertrand Girard,[a] Greg O. Sitz,[b] and Richard N. Zare
Department of Chemistry, Stanford University, Stanford, California 94305

Nicolas Billy and Jacques Vigué[a]
Laboratoire de Spectroscopie Hertzienne de l'E.N.S.,[c] 24 rue Lhomond, 75231 Paris Cedex 05, France

(Received 20 December 1991; accepted 16 March 1992)

The $(2+2)$ resonance-enhanced multiphoton ionization (REMPI) of N_2 via the $a\,^1\Pi_g(v=1,J)$ levels shows a strong dependence on the polarization of the laser beam causing this process. This behavior is attributed to the ac Stark effect produced by the near resonance of the N_2 $o_3\,^1\Pi_u(v=0,J)$ levels with the sum of the first three photons. The multiphoton transitions are broadened and asymmetric in appearance; one level is even split. The line profiles change markedly as the polarization of the laser beam is varied from linear to circular. A general theory is presented for the ac Stark effect in a diatomic molecule undergoing a multiphoton transition. When the sum of the photon energies is resonant with an allowed transition, a splitting of the line is observed (Autler–Townes effect). Off resonance, the magnetic sublevels are shifted by different amounts, causing the line profile to be broadened and distorted. This theoretical treatment is able to explain in a satisfactory manner the observed behavior of $(2+2)$ REMPI of N_2 via the $a\,^1\Pi_g$–$X\,^1\Sigma_g^+$ transition and the two-photon laser-induced fluorescence of CO via the $A\,^1\Pi$–$X\,^1\Sigma^+$ transition.

I. INTRODUCTION

Perturbations in molecular spectra appear as deviations in an expected pattern of line positions.[1] Often perturbed lines show sharp intensity variations as well as changes in the linewidths. These characteristics are independent of the polarization of the radiation source for a sample of randomly oriented molecules having no spatial anisotropy. Imagine then how puzzling it was to find in the $(2+2)$ resonance-enhanced multiphoton ionization (REMPI) of N_2 that the position, intensity, and profile of certain transitions varied markedly as the polarization was changed from linear to circular.[2] The clarification of these observations motivated this paper. This phenomenon is not a perturbation between interacting levels in the absence of radiation. Rather, it is caused by the interaction of the electromagnetic field with the molecular energy levels and may be regarded in that sense to be a perturbation between molecular energy levels "dressed" by the radiation field.

This phenomenon, first observed on a radio-frequency (rf) transition by Autler and Townes[3] in 1955, is called by many names, the ac Stark effect (our choice), the dynamic Stark effect, the Autler–Townes effect, and simply as the light shift. Its theory has been extensively developed[4] and experimental verifications in the radio-frequency and microwave regions of the electromagnetic spectrum are well known.[5] With the advent of powerful infrared (IR), visible, and ultraviolet (UV) lasers, specifically with the introduction of multiphoton absorption techniques, the ac Stark effect has regained interest, both as limiting the ultimate resolution of Doppler-free techniques and, in itself, as an interesting field of investigation for testing the fundamental theory of radiation–matter interactions.[6]

The first experimental observation of the ac Stark effect in the optical domain was obtained in 1966 by Aleksandrov *et al.*[7] in a double-resonance study of potassium vapor. Since then, extensive studies of Autler–Townes splittings[8] and ac Stark shifts[9] have been conducted by different groups on various atomic systems. Recently, the ac Stark effect has been used to produce subtle effects on the atomic system itself. For example, it plays a central role in laser cooling techniques below the Doppler limit (the so-called Sisyphus effect[10]). It has also been proposed to use the phase shift induced by the ac Stark effect on the wave function of an atomic system as a nondestructive technique for monitoring the intensity of an electromagnetic field.[11]

The importance of the ac Stark effect has been much less appreciated in experiments involving molecules. Although multiphoton absorption studies on molecules are common, the significance of light shifts in such experiments is often underestimated or ignored. A naive point of view is to assume that the ac Stark effect is small and disappears as the laser intensity is reduced. Although this view is true in most experiments involving a simple three-level system,[12] it fails when a fourth level is introduced, as we show. Moreover, the light shifts of molecular transitions may exhibit a strong polarization dependence, a fact that may surprise the uninitiated and that needs to be taken into account in interpreting

[a] Present address: Laboratoire de dynamique des édifices atomiques, IRSAMC, Université Paul Sabatier, 118 Route de Narbonne, 31062 Toulouse Cedex, France.
[b] Present address: Department of Physics, University of Texas, Austin, Texas 78712.
[c] Laboratoire associé au CNRS (U.A. 18), à l'Ecole Normale Supérieure et à l'Université Pierre et Marie Curie.

 0021-9606/92/130026-16$06.00

polarization measurements in terms of the orientation and alignment state multipoles of the molecule.[13]

The ac Stark effect has already been reported for molecular systems and analyzed in a few cases. In 1981, Otis and Johnson[14] found a marked narrowing of the ac Stark-broadened REMPI spectra of NO caused by increasing the pressure. At first, this was attributed to some collective effect[15] but later was shown to be likely the result of space–charge effects.[16] Quantitative analysis of the ac Stark effect in two-photon excitation spectra have been reported in CO (Ref. 17) and NO (Ref. 18). Light shifts have also been reported in the (2 + 1) REMPI of H_2 via its E,F state,[19–22] predicted in (1 + 1) autoionization of H_2,[23] and observed and analyzed in four-wave mixing in I_2 (Ref. 24) and N_2. (Ref. 25). We also call attention to a two-color study of the Autler–Townes splittings in the multiphoton ionization spectra of H_2, which has been proposed as a new technique for measuring transition dipole moments.[26] Finally, laser-induced level crossings in the dissociation of diatomic molecules have been theoretically investigated in the time domain.[27]

In this paper we review the general theory of the ac Stark effect for a diatomic molecule and apply it to the (2 + 2) REMPI of N_2 and to the two-photon induced fluorescence of CO. The ion yield as a function of wavelength reflects the resonant two-photon step, N_2 $a\,{}^1\Pi_g(v'=1,J')$–$X\,{}^1\Sigma_g^+(v''=0,J'')$. Several O- and P-branch transitions appear asymmetrically broadened and the $O(20)$ line appears to be split into two broad features in linear polarization but only slightly broadened in circular polarization. A quantum treatment of the ac Stark effect is able to reproduce successfully the observed REMPI spectrum as a function of polarization. The asymmetric broadening is caused by the ac Stark effect produced by the N_2 $o_3\,{}^1\Pi_u(v=0)$ state that is nearly resonant with the energy sum of the first three photons. The splitting observed on the $O(20)$ line is shown to be the result of almost exact resonance with the $R(18)$ line of the N_2 $o_3\,{}^1\Pi_u$–$a\,{}^1\Pi_g$ (0,1) band. The ac Stark effect produces an asymmetric broadening in the two-photon laser-induced fluorescence of the CO $A\,{}^1\Pi$ state. This case illustrates the nonresonant ac Stark effect presented in the theoretical part and we show how this broadening varies linearly with the laser power.

II. PHENOMENOLOGICAL TREATMENT

This short section contains largely review material that allows the connection to be made between classical and quantum descriptions of the ac Stark effect. In describing classically the interaction of matter on an electromagnetic field, it is useful to introduce a complex quantity called the index of refraction. The imaginary part of the index of refraction expresses the gain or loss of photons, i.e., the emission or absorption of radiation. The real part of the index of refraction describes an alteration in the propagation velocity of the electromagnetic field but with no change in the number of photons. The corresponding perturbation of matter by this altered electromagnetic field gives rise to light shifts, Autler–Townes splittings, and what we call collectively the ac Stark effect. Because the total energy is conserved, the energy change in the electromagnetic field must balance the energy change in the matter system. Therefore, the light shift of the ground state can be directly deduced from the linear susceptibility of the medium at the frequency of the electromagnetic field,[5(b)] as is shown in what follows.

The energy density of a monochromatic electromagnetic field of angular frequency $\omega = 2\pi\nu$ is given by the average (over a cycle) of the scalar product of the electric field $\mathbf{E} = \mathbf{E}_0 \cos \omega t$ and the polarization $\mathbf{P} = \epsilon_0 n_\omega \mathbf{E}$ of the medium, where ϵ_0 is the vacuum permittivity and n_ω is the index of refraction at ω. This yields $\frac{1}{2}\epsilon_0 n_\omega |\mathbf{E}_0|^2$. In the general case (at a value of ω far away from internal resonance of the matter system), n_ω may be approximated by a real quantity greater than unity. Thus, the energy density of the electromagnetic field increases upon entering the medium and decreases upon leaving it. The energy change of the electromagnetic field in the medium is a positive quantity, given by

$$\Delta E_{\text{field}} = \tfrac{1}{2}\epsilon_0 (n_\omega - 1)|\mathbf{E}_0|^2. \tag{1}$$

It is simply caused by the slowing down of the photons inside the medium, which increases the density of photons (the energy of each photon and the number of photons remaining constant in this case). As the index of refraction approaches unity (ω distant from the angular frequency of any absorption line), n_ω is given by $n_\omega = [1 + \chi^{(1)}]^{1/2} \simeq 1 + \frac{1}{2}\chi^{(1)}$, where $\chi^{(1)}$ is the linear susceptibility, given by[28]

$$\chi^{(1)} = \frac{N}{\epsilon_0} \sum_n |\mathbf{d}_{ng}\cdot\boldsymbol{\epsilon}|^2 \left[\frac{1}{\hbar(\omega_{ng} - \omega)} + \frac{1}{\hbar(\omega_{ng} + \omega)}\right]. \tag{2}$$

Here n represents any excited state of the system, ω_{ng} is the angular transition frequency between n and g, $\mathbf{d}_{ng}$ is the transition dipole moment, $\boldsymbol{\epsilon}$ is the polarization unit vector of the electromagnetic field, and N is the number density of matter systems (atoms, molecules, etc.). The energy change ΔE_{field} is balanced by an opposite energy change in the ground state of the matter system, i.e.,

$$\Delta E_g = -\Delta E_{\text{field}}/N = -\frac{1}{2\hbar} \sum_n |\mathbf{d}_{ng}\cdot\mathbf{E}_0|^2 \frac{\omega_{ng}}{\omega_{ng}^2 - \omega^2}. \tag{3}$$

Hence, Eq. (3) is the phenomenological expression for the light shift of the ground state in the nonresonant case. In what follows, we use a more rigorous formalism to establish a general formula of the light shift for any internal state of a quantized matter system, at or away from resonance.

III. QUANTUM TREATMENT

The dressed-state formalism is well suited to express the mutual interaction between an electromagnetic field and a quantum system.[29] In this formalism, both the electromagnetic field and the matter system are quantized; their interaction is studied in the Hilbert space resulting from the direct product of the Hilbert space of the electromagnetic field and the Hilbert space of the matter system. The states of this new Hilbert space are of the type $|i,n\rangle$, where $|i\rangle$ is a state of the matter system and $|n\rangle$ is a state of the electromagnetic field. The total Hamiltonian of the system is

$$H = H_{\text{matter}} + H_{\text{rad}} + H_{\text{int}}, \tag{4}$$

where H_{matter}, H_{rad}, and H_{int} are, respectively, the Hamiltonians of the matter system, the electromagnetic field, and the interaction between them. In the electric dipole approximation, the latter is represented by[29]

$$H_{\text{int}} = -\mathbf{D}\cdot\mathbf{E}(\mathbf{r}), \tag{5}$$

where $\mathbf{D}$ is the electric dipole operator of the matter system and $\mathbf{E}(\mathbf{r})$ is the electric field operator of the electromagnetic field. Specifically,

$$\mathbf{E}(\mathbf{r}) = i(\hbar\omega/2\epsilon_0 V)^{1/2}(\boldsymbol{\epsilon} a e^{i\mathbf{k}\cdot\mathbf{r}} - \boldsymbol{\epsilon}^* a^+ e^{-i\mathbf{k}\cdot\mathbf{r}}), \tag{6}$$

where a^+ and a are the creation and annihilation operators associated with the normal mode $\boldsymbol{\epsilon}$ of the electromagnetic field, $\mathbf{k}$ is the wave vector, and V is the quantization volume of the field. For simplicity, we assume in Eq. (6) that the electric field is in a normal mode so that the radiation is either linearly, left or right-circularly polarized. The generalization to an elliptical polarization is straightforward; it consists of summing over the different possible modes in Eq. (6).

Consider two state $|e\rangle$ and $|i\rangle$ of the quantized matter system. Then the matrix elements of H_{int} connecting them are readily deduced from the well-known properties of a^+ and a,[30]

$$H_{ie,+} = \langle i,n+1|H_{\text{int}}|e,n\rangle = -i[(n+1)\hbar\omega/2\epsilon_0 V]^{1/2}\langle i|\mathbf{D}\cdot\boldsymbol{\epsilon}^*|e\rangle e^{-i\mathbf{k}\cdot\mathbf{r}} \tag{7a}$$

and

$$H_{ie,-} = \langle i,n-1|H_{\text{int}}|e,n\rangle = -i[n\hbar\omega/2\epsilon_0 V]^{1/2}\langle i|\mathbf{D}\cdot\boldsymbol{\epsilon}|e\rangle e^{i\mathbf{k}\cdot\mathbf{r}}. \tag{7b}$$

We introduce the notation $\hbar\omega_{ie} = E_i - E_e$, the energy difference between the $|i\rangle$ and $|e\rangle$ levels of the quantized matter system. For simplicity, we suppose that ω_{ie} is positive, i.e., $E_i \geqslant E_e$. The matter–radiation levels coupled by H_{int} have an energy difference of either $\hbar(\omega_{ie}+\omega)$ or $\hbar(\omega_{ie}-\omega)$. To first order the effect of H_{int} is to mix the $|e,n\rangle$ and $|i,n\pm1\rangle$ states, inducing a virtual transition between $|e\rangle$ and $|i\rangle$. The light shift is a second-order correction to the energy levels associated with the states $|e,n\rangle$ and $|i,n\pm1\rangle$. The light shift can also be regarded as resulting from two consecutive virtual transitions, absorption followed by emission, or emission followed by absorption. Two important cases can then be distinguished depending on the relative magnitudes of $H_{ie,\pm}$ and $\hbar(\omega_{ie}\pm\omega)$.

A. Nondegenerate case: Quadratic ac Stark effect

When the energy difference $\hbar(\omega_{ie}\pm\omega)$ of the states coupled by H_{int} is much larger than the magnitudes of the matrix elements of H_{int} causing this coupling, the light shift of the level $|e\rangle$ may be estimated from second-order perturbation theory

$$\Delta E_e = -\left[\frac{|H_{ie,+}|^2}{\hbar(\omega_{ie}+\omega)} + \frac{|H_{ie,-}|^2}{\hbar(w_{ie}-\omega)}\right]. \tag{8}$$

The generalization of this expression to a multilevel system is obtained by summing over all the different possible states $|i\rangle$ connected to $|e\rangle$. Moreover, the energy correction to the level $|i\rangle$ is just obtained by interchanging the labels e and i. With the approximation $(n+1)^{1/2} \simeq n^{1/2}$, which is always valid for the high-energy fluxes used in multiphoton experiments, we obtain

$$\Delta E_e = -\frac{P}{\epsilon_0 cS\hbar}\sum_i |\langle i|\mathbf{D}\cdot\boldsymbol{\epsilon}|e\rangle|^2 \frac{\omega_{ie}}{\omega_{ie}^2-\omega^2}, \tag{9}$$

where we have replaced $n\hbar\omega/V$ by P/Sc, with c the speed of light, P the total power of the electromagnetic field (laser beam), and S its cross section. Equation (9) is seen to be identical to Eq. (3) by recognizing that the modulus of the Poynting vector P/S equals $\frac{1}{2}\epsilon_0 c E_0^2$. This provides a quantum justification for the classical arguments used to derive Eq. (3).

Equation (9) shows that ΔE_e varies quadratically with the electric field strength of the electromagnetic wave (the quadratic ac Stark effect). Hence, ΔE_e is linear in the power density. Note that the sign of this light shift may change when the angular frequency ω crosses an absorption line with angular frequency ω_{ie}. Note that for the ground state $|g\rangle$ ω_{ig} is always positive for any i. Hence, if ω is less than any angular absorption frequency of the system, the light shift ΔE_g is negative for the ground state; again, this result is in agreement with Eq. (3). In particular, when $\omega = 0$, we find that Eq. (9) reduces to the well-known quadratic dc Stark effect.

By analogy with the operator used to describe a two-photon transition,[12,31] light shift operators Δ_+ and Δ_- may be defined by

$$\Delta_+ = -\sum_i \mathbf{D}\cdot\boldsymbol{\epsilon}\frac{|i\rangle\langle i|}{\hbar(\omega+\omega_{ie})}\mathbf{D}\cdot\boldsymbol{\epsilon}^* \tag{10a}$$

and

$$\Delta_- = \sum_i \mathbf{D}\cdot\boldsymbol{\epsilon}^*\frac{|i\rangle\langle i|}{\hbar(\omega-\omega_{ie})}\mathbf{D}\cdot\boldsymbol{\epsilon}. \tag{10b}$$

In Eq. (10a) Δ_+ describes the ac Stark effect arising from a virtual absorption of a photon of angular frequency ω followed by a virtual stimulated emission of a photon at the same angular frequency; in Eq. (10b) Δ_- corresponds to the reverse process. Then Eq. (9) can be rewritten as

$$\Delta E_e = \frac{P}{2\epsilon_0 cS\hbar}[\langle e|\Delta_+|e\rangle + \langle e|\Delta_-|e\rangle], \tag{11}$$

from which it is apparent that the diagonal matrix elements of $\Delta_\pm$ are the light shifts. The off-diagonal matrix elements, $\langle e'|\Delta_\pm|e\rangle$, describe an effective transfer from the state $|e\rangle$ to the state $|e'\rangle$. In this process, the number of photons in the electromagnetic field remains unchanged. Conservation of energy requires that $|e\rangle$ and $|e'\rangle$ lie at the same energy; this process, in which $|e\rangle$ and $|e'\rangle$ are coupled without the creation or destruction of photons, is the well-known photocatalytic effect, studied in detail by Lau.[32]

B. Quasidegenerate case: Linear ac Stark effect

For $\hbar(\omega_{ie}-\omega) \lesssim |H_{ie,\pm}|$, perturbation theory cannot be used and an exact diagonalization must be performed. In

general, only one level $|i\rangle$ satisfies this condition and the contributions of all other levels can often be neglected. Furthermore, the nonresonant contributions of $H_{ie,+}$ can be neglected in most cases and the light shift calculation reduces to the diagonalization of a two-level system. The new energy levels E_+ and E_- are given by

$$E_\pm = \hbar\left\{\frac{\omega_e+\omega_i+\omega}{2} \pm \frac{1}{2}\left[(\omega_{ie}-\omega)^2+4|H_{ie,\pm}|^2/\hbar^2\right]^{1/2}\right\}. \quad (12)$$

In the limit of exact resonance, $\omega_{ie}=\omega$, or very high electromagnetic field strength, $\hbar(\omega_{ie}-\omega) \ll |H_{ie,\pm}|$, Eq. (12) reduces to the linear ac Stark effect,

$$E_\pm = \hbar\left(\frac{\omega_e+\omega_i+\omega}{2}\right) \pm |H_{ie,\pm}|, \quad (13)$$

and the new eigenstates are the symmetric and antisymmetric combinations of the original states in the absence of interaction,

$$|\psi_\pm\rangle = \frac{1}{\sqrt{2}}(|i,n-1\rangle \pm |e,n\rangle). \quad (14)$$

Two important features characterize this case. (1) The energy splitting, which is directly connected to the Rabi frequency of the $(i \leftarrow e)$ transition, is proportional to the electric field, and hence to the square root of the laser power, and (2) if one of the levels, for example the $|e\rangle$ level, is connected to another level $|g\rangle$ by an electric dipole transition, then the emission (or absorption) will be split into two lines, one line connected to the $|\psi_+\rangle$ level, the other connected to the $|\psi_-\rangle$ level. Each line has equal intensity and carries half of the total intensity. This is the well-known Autler–Townes effect.[3]

C. Application to diatomic molecules

The application of the general theory presented above to diatomic molecules requires the evaluation of the matrix elements of $H_{\rm int}$ in a molecular basis set. This requires the evaluation of the scalar product $\mathbf{D}\cdot\boldsymbol{\epsilon}$, where the electric field $\boldsymbol{\epsilon}$ is naturally most easily evaluated in the laboratory frame and the electric dipole moment $\mathbf{D}$ in the molecular frame. This problem is easily solved using Wigner rotation matrices.[33,34] We will treat it in a Hund's case (a) basis set, which applies to molecular states of N_2. The extension to any other coupling case is straightforward through a similar treatment.

We first expand $\mathbf{D}\cdot\boldsymbol{\epsilon}$ in the laboratory frame,

$$\mathbf{D}\cdot\boldsymbol{\epsilon} = \sum_q (-1)^q \epsilon^{(1)}_{-q} D^{(1)}_q, \quad (15)$$

where $\epsilon^{(1)}_{-q}$ and $D^{(1)}_q$ are the standard components of the electric field and electric dipole moment of the molecule in the laboratory frame. Using the Wigner rotation matrix $D^{(1)}_{q,n}(\phi,\theta,\chi)$ between the molecular and laboratory frames, where ϕ,θ,χ describe the three Euler angles connecting the two frames, we write

$$D^{(1)}_q = \sum_n D^{(1)*}_{q,n}(\phi,\theta,\chi) d^{(1)}_n. \quad (16)$$

Here $d^{(1)}_n$ designates the components of the dipole moment in the molecular frame. The matrix elements of $\mathbf{D}\cdot\boldsymbol{\epsilon}$ in the molecular basis set $|v,\Lambda,s,\Sigma;J,\Omega,M\rangle$ are then calculated,

$$\langle i|\mathbf{D}\cdot\boldsymbol{\epsilon}|e\rangle = \sum_q (-1)^q \epsilon^{(1)}_{-q} \times \sum_n \langle i,v_i,\Lambda_i,s_i,\Sigma_i|d^{(1)}_n|e,v_e,\Lambda_e,s_e,\Sigma_e\rangle \times \langle J_i,\Omega_i,M_i|D^{(1)*}_{q,n}(\phi,\theta,\chi)|J_e,\Omega_e,M_e\rangle, \quad (17)$$

where we have neglected any dependence of the transition dipole matrix elements on the rotation quantum number, which is usually a very good approximation (so long as the rotational energy is small compared to the vibrational spacing). The second matrix element of Eq. (17) completely expresses the rotational and angular dependence. It is given by[35,36]

$$\langle J_i,\Omega_i,M_i|D^{(K)*}_{q,n}(\phi,\theta,\chi)|J_e,\Omega_e,M_e\rangle = (-1)^{M_i-\Omega_i}[(2J_i+1)(2J_e+1)]^{1/2} \times \begin{pmatrix} J_i & K & J_e \\ -M_i & q & M_e \end{pmatrix}\begin{pmatrix} J_i & K & J_e \\ -\Omega_i & n & \Omega_e \end{pmatrix}. \quad (18)$$

As expected from the comparison with the dc Stark effect, the ac Stark effect clearly splits the degeneracy of the different magnetic sublevels. The M dependence of $\langle i|\mathbf{D}\cdot\boldsymbol{\epsilon}|e\rangle$ is given in Table I for the standard polarizations. Recall that the ac Stark shift varies either quadratically (Sec. III A) or linearly (Sec. III B) with this matrix element. Therefore, a splitting of the absorption (or emission) lines into J or $J+1$ components (linear polarization) or $2J+1$ components (circular polarization) should be expected. However, this is seldom the case in practice. Because of the variation of the laser power density across the laser profile, the line shape is in fact inhomogeneously broadened. Moreover, different other sources of broadening (such as the laser spectral profile and the Doppler profile) will in general mix these components and prevent the observation of such magnetic sublevel splittings. We present a study of all these effects in more detail in the next section.

Overall, the intensity of each Zeeman component depends on the way it is observed. For instance, in a laser-induced fluorescence (LIF) experiment, the intensity of each Zeeman component of the line depends on its excitation and detection probability, which depends sensitively on the polarization of the laser and on the nature of the excitation

TABLE I. Angular dependence of the matrix element $\langle i, J_i, M_i|\mathbf{D}\cdot\boldsymbol{\epsilon}|e, J_e, M_e\rangle$.

Branch	Polarization	
	Circular	Linear
P	$[(J_e-M_e)(J_e-M_e-1)]^{1/2}$	$[J_e^2-M_e^2]^{1/2}$
Q	$[(J_e-M_e)(J_e+M_e+1)]^{1/2}$	M_e
R	$[(J_e+M_e+1)(J_e+M_e+2)]^{1/2}$	$[(J_e+1)^2-M_e^2]^{1/2}$

line (O,P,Q,R,S branch, etc.) as well as on the location of the detector with respect to the polarization of the laser.[37] As these effects are special to the experiment performed, we will only detail them in each experimental case studied here.

Before closing this section, we show how the ac Stark effect for a diatomic molecule takes on a simple form far from resonance. With the help of Eq. (17), the matrix elements of the light shift operator Δ_+ may be written as

$$\langle e|\Delta_+|e'\rangle = -\sum_{q,q'}(-1)^{q+q'}(\epsilon^*)^{(1)}_q\epsilon^{(1)}_{q'}$$
$$\times\sum_{n,n'}\sum_i\langle e,v_e,\Lambda_e,S_e,\Sigma_e|d^{(1)}_n|i,v_i,\Lambda_i,S_i,\Sigma_i\rangle\langle i,\Lambda_i,S_i,\Sigma_i|d^{(1)}_{n'}|e',v'_e,\Lambda'_e,S'_e,\Sigma'_e\rangle$$
$$\times\sum_{J_i,\Omega_i,M_i}\frac{\langle J_e,\Omega_e,M_e|D^{(1)*}_{q,n}(\phi,\theta,\chi)|J_i,\Omega_i,M_i\rangle\langle J_i,\Omega_i,M_i|D^{(1)*}_{q',n'}(\phi',\theta',\chi')|J'_e,\Omega'_e,M'_e\rangle}{\hbar[\omega+\omega_i(v_i,\Lambda_i,J_i)]}, \tag{19}$$

with a corresponding expression for $\langle e|\Delta_-|e'\rangle$. In Eq. (19) the summation over J_i is limited to three terms, $J_i = J_e$ and $J_i = J_e \pm 1$. Far from resonance the variation of the energy denominator with J_i in Eq. (19) can be neglected so that it can be factored out as a constant; moreover, the time spent in the intermediate state, $2\pi/(\omega-\omega_i)$, is small compared to the classical period of rotation in the intermediate state, $\hbar/2BJ_i$, so that the angular arguments of the two rotation matrices in Eq. (19) may be approximated as the same. Then, use of the closure relation

$$\sum_{J_i,\Omega_i,M_i}|J_i,\Omega_i,M_i\rangle\langle J_i,\Omega_i,M_i| = I \tag{20}$$

and the Clebsch–Gordan series for the product of two Wigner rotation matrices with the same Euler-angle arguments,[36] allows the light shift operator to be recast in the form

$$\Delta_+ = \sum_{K,Q,N}(a_+)^{(K)}_Q(\delta_+)^{(K)}_N D^{(K)}_{Q,N}(\phi,\theta,\chi), \tag{21}$$

where

$$(a_+)^{(K)}_Q = \sum_{q,q'}(\epsilon^*)^{(1)}_{-q}(\epsilon)^{(1)}_{q'}(2K+1)^{1/2}\begin{pmatrix}1 & 1 & K\\ q & q' & -Q\end{pmatrix} \tag{22}$$

contains all the polarization factors,

$$(\delta_+)^{(K)}_N = -\sum_{n,n',i}(-1)^N(2K+1)^{1/2}$$
$$\times\begin{pmatrix}1 & 1 & K\\ n & n' & -N\end{pmatrix}\frac{d^{(1)}_n|i\rangle\langle i|d^{(1)}_{n'}}{\hbar(\omega+\omega_i)} \tag{23}$$

contains all the electric dipole transition moment factors, and $D^{(K)}_{Q,N}(\phi,\theta,\chi)$ is a Wigner rotation matrix element of rank K, where in Eqs. (21)–(23) K ranges from 0 to 2 in unit steps. A similar expression to Eq. (21) holds for Δ_-, where $(a_-)^{(K)}_Q$ is obtained from $(a_+)^{(K)}_Q$ by exchanging ϵ and ϵ^*, and $(\delta_-)^{(K)}_N$ is obtained from $(\delta_+)^{(K)}_N$ by replacing ω with $-\omega$.

Note that the $|\Lambda,S,\Sigma;J,\Omega,M\rangle$ basis vectors used in this calculation are not in general eigenvectors of the molecule, even if the molecule obeys Hund's case (a) coupling. In particular, for states with $\Lambda\neq 0$ (or $\Omega\neq 0$), the eigenvectors are symmetric and antisymmetric linear combinations of $|\Lambda\rangle$ and $|-\Lambda\rangle$ states. It is therefore necessary in general to calculate two types of matrix elements, $\langle\Lambda|(\delta_\pm)^{(K)}_N|\Lambda\rangle$ and $\langle\Lambda|(\delta_\pm)^{(K)}_N|-\Lambda\rangle$.

The calculation of the ac Stark effect far from resonance is readily carried out using Eqs. (21)–(23) by expressing a given molecular state in the $|\Lambda,S,\Sigma;J,\Omega,M\rangle$ basis set. We limit our analysis to Hund's case (a). If we define

$$A(\Omega,\Omega') = \langle\Lambda,S,\Sigma;J,\Omega,M|(\Delta_+ + \Delta_-)|\Lambda',S,\Sigma';J',\Omega',M'\rangle, \tag{24}$$

then for symmetry reasons $A(\Omega,\Omega') = A(-\Omega,-\Omega')$. It follows that only two matrix elements need to be calculated in the most general case, $A(\Omega,\Omega')$ and $A(\Omega,-\Omega')$. However, because of the $|\Delta\Omega|\leqslant 2$ selection rule, it is only necessary to calculate explicitly these two terms for the case $|\Omega| = |\Omega'| = 1$. The application of Eq. (21) will be illustrated in Sec. V, which discusses the ac Stark effect in the two-photon (LIF) of CO.

IV. (2+2) REMPI SPECTRUM OF N_2

A. Experimental data

1. Apparatus

The experiments described here have been performed in the course of a gas–surface scattering study of N_2 on Ag(111).[38–41] The N_2 molecules were detected in a quantum-state-specific manner by (2 + 2) REMPI. The apparatus has already been described in detail. We review only its main features. Some of the data presented here have been obtained with surface-scattered N_2, other with the chamber uniformly filled with static N_2 at a pressure of 5×10^{-7} Torr. No qualitative difference was observed in the ac Stark effect for these two operating conditions. The tunable radiation used to excite the (1,0) band of the N_2 $a\,^1\Pi_g$–$X\,^1\Sigma_g^+$ transition at $\lambda = 283$–285 nm was generated by frequency doubling the output of a Nd^{+3}:YAG-pumped dye laser (Quantel YGC581C-TDL50-UVX2). Typical energies were 13–16 mJ/pulse at 283 nm, measured at the entrance of the chamber. The polarization of the laser light was controlled with half and quarter-wave plates (Special Optics).

The wave plates were zero-order plates, air-spaced, and antireflection coated. The laser beam was focused between the grids of a time-of-flight mass spectrometer by a 250 mm focal length AR-coated lens.

Ions formed at the laser focus were collected in a time-of-flight mass spectrometer and detected with a multichannel plate (Galileo CEMA).[42] Ion signal collection, laser wavelength, and laser polarization were all computer controlled via a CAMAC interfaced to a DEC PDP 11/23 computer.

2. Results

The ion signal was found to vary with the square of the laser power,[2] in agreement with an independent study.[43] Moreover, when background N_2 was probed, it was verified that correction of the line intensities by the nuclear spin degeneracy and by the rotational line strength of the N_2 $a\,^1\Pi_g$–$X\,^1\Sigma_g^+$ two-photon transition[44–47] gave a room-temperature Boltzmann distribution. These two observations indicate that the strongly nonresonant two-photon excitation of the $a\,^1\Pi_g$ state is the rate limiting step in this $(2+2)$ REMPI detection scheme and that the two subsequent steps are completely saturated.

Figure 1 shows a typical $(2+2)$ REMPI spectrum of room-temperature N_2 obtained at a pressure of 5×10^{-7} Torr. The relative ion intensity is plotted as a function of the dye laser wavelength. Rotational lines belonging to the *O*, *P*, and *S* branches are identified. The *Q*-branch lines are very weak and most of the *R*-branch lines are overlapped [between the $S(0)$ and $P(2)$ lines]. The bandhead, which appears at $\lambda\simeq569.5$ nm, corresponds to $(3+1)$ REMPI through the $v=6$ level of the N_2 $b\,^1\Pi_u$ state (see, for example, Ref. 48). Note the odd–even alternation of the line intensities, caused by nuclear spin statistics in this homonuclear diatomic molecule ($I=1$ for ^{14}N).

The most interesting features appear between 567.9 and 569 nm. Lines of the *P* branch show an asymmetric broadening, which increases from $P(18)$ to $P(21)$ and then changes sign at $P(22)$ [with a width comparable to $P(21)$]. Lines of the *O* branch present still more striking features. The $O(16)$–$O(19)$ and $O(21)$–$O(23)$ lines are asymmetrically broadened similar to the $P(18)$–$P(21)$ and $P(22)$ lines. No line is observed at the expected position of the $O(20)$ line, which should be midway between two broad bumps. These broad bumps are asymmetric with opposite signs. The scattering of N_2 on an Ag(111) surface is known to produce highly aligned molecules with **J** perpendicular to the surface normal.[38] This feature was used to measure the alignment of these two bumps. Both exhibited alignment characteristic of a $\Delta J=\pm2$ transition (very different from a $\Delta J=\pm1$ transition) and similar to the alignment of the neighboring $O(19)$ and $O(21)$ lines. This allowed an assignment of these bumps as two parts of the $O(20)$ line.

These observations suggested at first that the $a\,^1\Pi_g$ state is perturbed near $v=1, J=18$ for the *e* component and near $v=1, J=20$–21 for the *f* component. Vanderslice *et al.*[49] made no mention of any perturbed lines in their absorption study of this band of N_2. However, owing to the weakness of this electric-dipole-forbidden transition, the $O(20)$ line was the last line they observed and its splitting may have been missed. However, this interpretation is not consistent with the following observations.

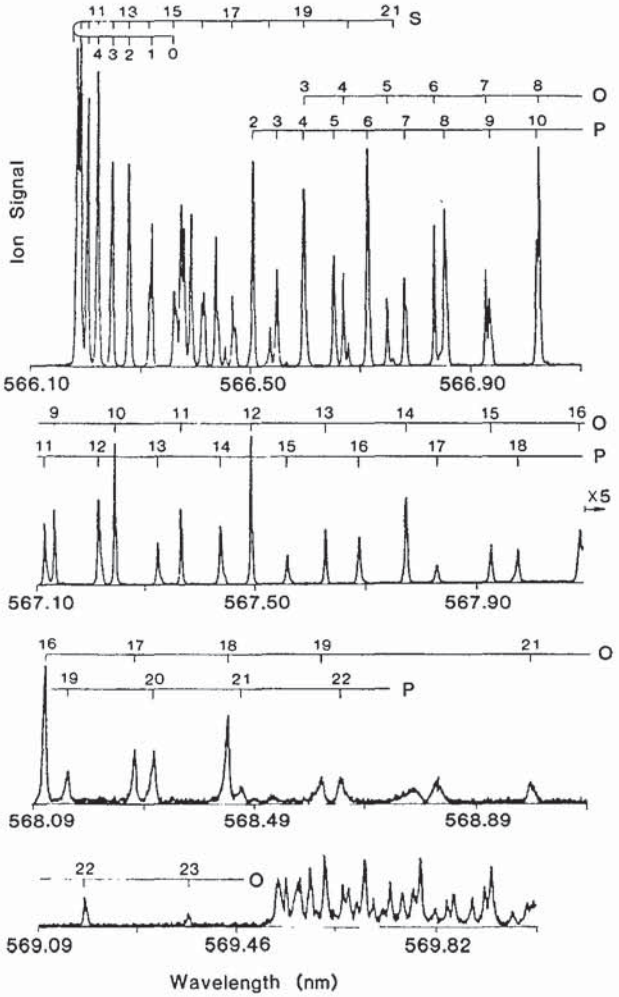

FIG. 1. $(2+2)$ REMPI spectrum of N_2 via the $a\,^1\Pi_g, v=1$ intermediate state. The lines of the *O*, *P*, and *S* branches are identified. Note the asymmetric broadening of the last lines of the *O* and *P* branches and the two bumps that appear at the expected place of the $O(20)$ line.

Figure 2 presents the profile of the $O(20)$ line obtained using different polarizations. The angle β describes the ellipticity of the laser beam. It corresponds to the angle between the optical axis of the quarter-wave plate and the polarization of the incoming beam. For linearly polarized light, $\beta=0°$, while for left/right circularly polarized light, $\beta=\pm45°$; intermediate values of β correspond to elliptically polarized light. As the polarization is varied from linear to circular, Fig. 2 shows that the line profile changes dramatically. The two broad bumps observed for $\beta=0°$ gradually collapse to a single sharp line at $\beta=45°$. This single line appears slightly broadened compared to a "normal" line [for example, $O(12)$], which does not exhibit any shape variation with the laser polarization. The differences observed between opposite values of β are a consequence of the fact that these spectra have been obtained from surface-scattered N_2, which causes a high degree of orientation for the

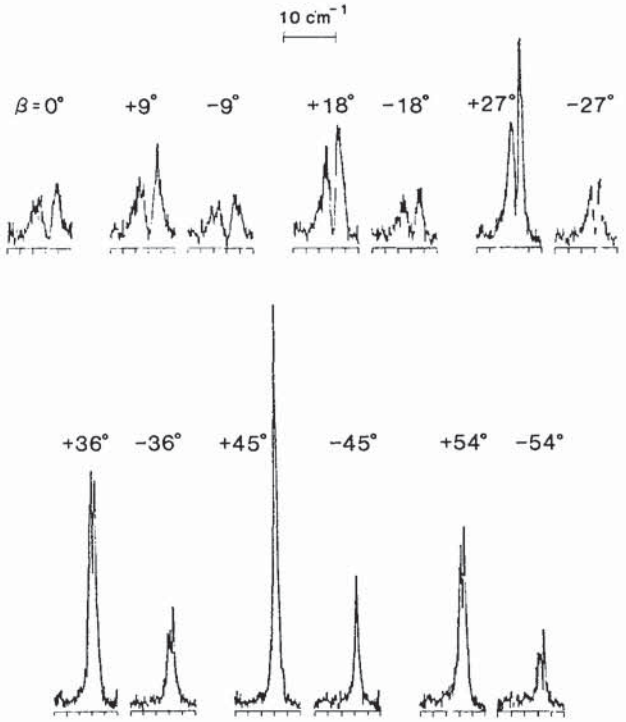

FIG. 2. Line shapes of the $O(20)$ line obtained with different laser polarization. β is the ellipticity of the laser beam; $\beta = 0°$ corresponds to linear polarization; $\beta = \pm 45°$ to circular polarization, intermediate angles to elliptic polarizations. These spectra were recorded with N_2 scattered from Ag(111) that is oriented (Ref. 39). This explains the lack of symmetry observed for opposite values of β. The horizontal scale corresponds to the laser frequency.

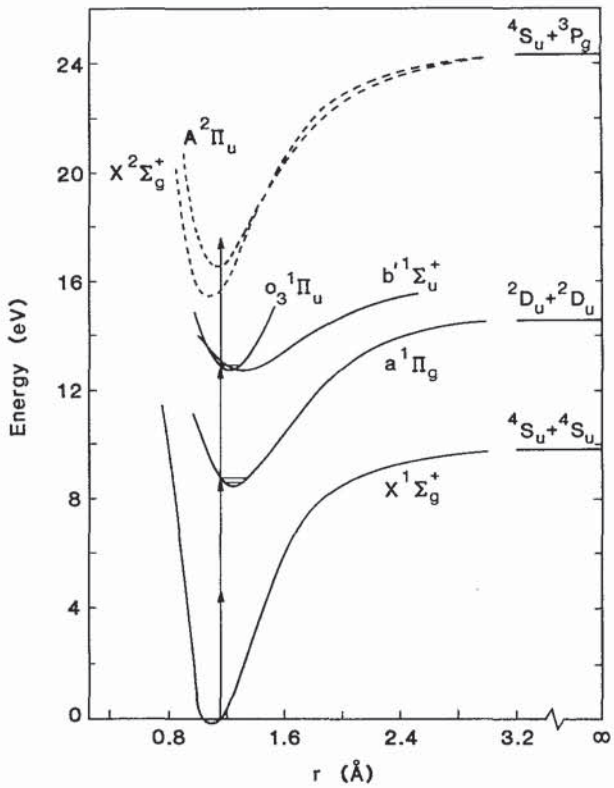

FIG. 3. Potential energy curves of the states of N_2 relevant to this study (Ref. 50).

highest rotational numbers.[39] Within experimental errors, these differences affect the intensity but not the line shape; this has been verified by examining neighboring lines.

3. Coupled states

The spectrum observed in a $(2+2)$ REMPI experiment reflects the absorption of the first two photons. The features observed here are therefore caused by a perturbation occurring either in the $X\,^1\Sigma_g^+$ ground state or the $a\,^1\Pi_g$ excited state. Note that the absorption of the first photon is totally nonresonant because there are no suitable intermediate states for this two-photon process. The ac Stark effect of the N_2 $X\,^1\Sigma_g^+$ state is therefore negligible. For the same reason, the ac Stark effect of the N_2 $a\,^1\Pi_g$ state can only be produced by a state lying at a higher energy, close to the energy of three photons above the ground state ($\simeq 13$ eV). At this energy, the density of Rydberg states of N_2 is high.[50] The N_2 $o_3\,^1\Pi_u$ $(v=0)$ (Ref. 51) and the N_2 $b'\,^1\Sigma_u^+$ $(v=3)$ (Refs. 48 and 52) states are two possible candidates (see Fig. 3). Figure 4 presents the photon energy of the N_2 $a\,^1\Pi_g$–$X\,^1\Sigma_g^+$ (1,0) two-photon transition as well as the N_2 $o_3\,^1\Pi_u$–$a\,^1\Pi_g$ (0,1) and N_2 $b'\,^1\Sigma_u^+$–$a\,^1\Pi_g$ (3,1) one-photon transitions. These energies are plotted as a function of the rotational quantum number of the N_2 $a\,^1\Pi_g$ state, J_a, which is common to these three transitions. This allows a direct graphical determination of the positions of the resonances. They occur for $J_a = 18$ between the O branch of the N_2 a–X transition and the R branch of the N_2 o_3–a transition, and between $J_a = 20$ and 21 for the P branch of the N_2

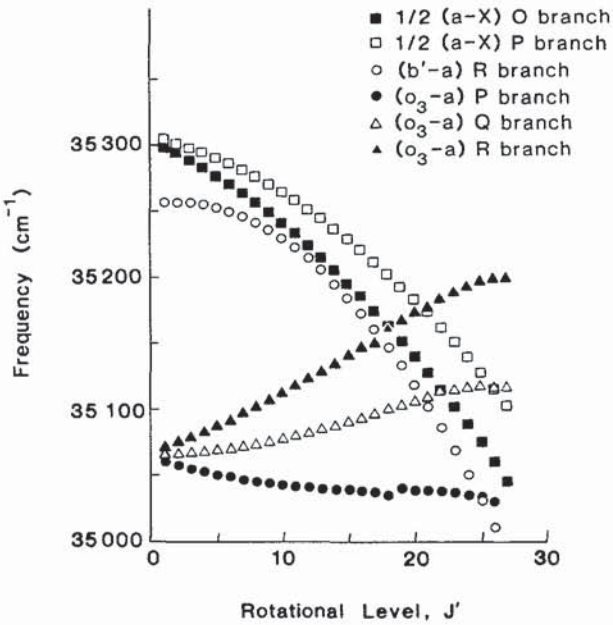

FIG. 4. Photon energies of the different transitions involved. Note that for two-photon transitions, half of the energy of the transition is plotted.

a–X transition and the R branch of the N_2 o_3–a transition. For the $O(20)$ line, the energy mismatch is only 0.26 cm^{-1}! These resonances match exactly the observations described above, the splitting of the $O(20)$ line and the change in the sign of the asymmetry between the $P(21)$ and $P(22)$ lines. No resonance occurs between the N_2 b'–a (3,1) and the N_2 a–X (1,0) transitions. The energy difference is close to 10 cm^{-1} between the N_2 b'–a (3,1) R branch and the N_2 a–X (1,0) O branch for the rotational levels $J = 10$–17. The transition dipole moment of the N_2 b'–a transition and the Franck–Condon factor for the (3,1) band are unknown. The transition dipole moment of this transition is not expected to be small, since the transition involves the excitation of only one electron. However, this transition appears never to have been observed. The $O(10)$ line exhibits little or no broadening. Therefore, it is likely that the Franck–Condon factor for the (3,1) band is small, and the contribution of the N_2 $b\,^1\Sigma_u^+$ state to the ac Stark effect of the N_2 $a\,^1\Pi_g$ state can be neglected.

B. Simulation of observed line profiles

1. Intensity of individual magnetic sublevels

As already indicated, it is a good assumption to consider that every N_2 molecule that can reach the resonant intermediate state N_2 $a\,^1\Pi_g$ becomes ionized, with a probability independent of the rotational level and that we also assume to be independent of the magnetic sublevel M. The intensity of each magnetic sublevel is therefore completely accounted for by the two-photon absorption probability. These probabilities are usually given without detailing the contribution of each magnetic sublevel,[44–46] but these can be easily obtained using the same methods and avoiding the M summation.[47] We simply recall the result here

$$\Gamma_g(J_g,M_g) = \left(\frac{P}{Sc}\right)^2 \frac{1}{\hbar^2\epsilon_0^2\Delta\omega_L} \times \sum_{K,Q,N} |\langle J_e,\Omega_e,M_e|D^{(K)*}_{Q,N}(\phi,\theta,\chi) \times |J_g,\Omega_g,M_g\rangle|^2 |a_Q^{(K)}\langle e|q_N^{(K)}|g\rangle|^2, \quad (25)$$

where

$$a_Q^{(K)} = \sum_{q,q'} (-1)^Q \epsilon_q^{(1)} \epsilon_{q'}^{(1)} \begin{pmatrix} 1 & 1 & K \\ q & q' & Q \end{pmatrix}, \quad (26)$$

$$\langle e|q_N^{(K)}|g\rangle = (-1)^N \sum_{n,n'} \begin{pmatrix} 1 & 1 & K \\ n & n' & N \end{pmatrix} \times \sum_i \frac{\langle e|d_n^{(1)}|i\rangle\langle i|d_{n'}^{(1)}|g\rangle}{\hbar(\omega-\omega_{ig})}, \quad (27)$$

and $D^{(K)*}_{Q,N}(\phi,\theta,\chi)$ is the Wigner rotation matrix of order K whose matrix elements have been given in Eq. (18). All the angular dependence of the two-photon absorption probability is contained in the matrix elements of the Wigner rotation matrix. In the case of standard polarization, the summation over Q reduces to one term, namely $Q = 0$ for linear polarization, ± 2 for circular polarization. The summation over N reduces also to one term, namely $N = \Omega_e - \Omega_g$. Finally, the irreducible tensorial operator $Q_0^{(0)}$ is nonvanishing only in the case of a Q-branch transition between states with the same Ω. This is not the case studied here; in our case, as in most of the cases, the summation over K,Q,N reduces to one term in which $K = 2$ and $N = 1$. Hence, the angular part can be completely factored from the two-photon probability.

Table II presents the high-J limit of this expression together with the most-populated magnetic sublevel for the lines of the different excitation branches (O,P,Q,R, and S), for linear and circular polarization. For linear polarization, the expression is independent of the sign of $\Delta J = J_e - J_g$, whereas for circular polarization, changing the sign of ΔJ is equivalent to changing $+M$ into $-M$. A comparison with Table I shows that, for both polarizations, when the line producing the light shift has the same ΔJ sign as the line of the two-photon excitation, the most shifted magnetic sublevels give rise to the strongest absorption. This is for example the case of a P-branch line ($\Delta J = -1$) producing the light shift when an O-branch line ($\Delta J = -2$) is used for the two-photon excitation (recall that an O-branch line is a succession of two P-branch transitions). In the case of linear polarization, this is also true for lines with the same value of $|\Delta J|$. Therefore, in the case of a light shift produced with linear polarization by an R-branch line after excitation by an O-branch line, it can be expected that the most intense levels undergo the largest shifts, giving rise to a large broadening. In contrast, with circular polarization the most shifted levels are the least intense, giving rise overall to a much smaller broadening. To illustrate this, Fig. 5 plots the intensity as

TABLE II. High-J limit of the angular dependence of the two-photon line strengths for a $\Delta\Omega \neq 0$ transition.

Branch	Polarization			
	Circular	M_{max}	Linear	M_{max}
O	$(J-M)^4/J^4$	$-J$	$6(J^2-M^2)^2/J^4$	0
P	$4(J-M)^3(J+M)/J^4$	$-J/2$	$24(J^2-M^2)M^2/J^4$	$\pm J/\sqrt{2}$
Q	$6(J^2-M^2)^2/J^4$	0	$4[3M^2-J(J+1)]^2/J^4$	$\pm J$,0
R	$4(J-M)(J+M)^3/J^4$	$J/2$	$24(J^2-M^2)M^2/J^4$	$J/\sqrt{2}$
S	$(J+M)^4/J^4$	J	$6(J^2-M^2)^2/J^4$	0

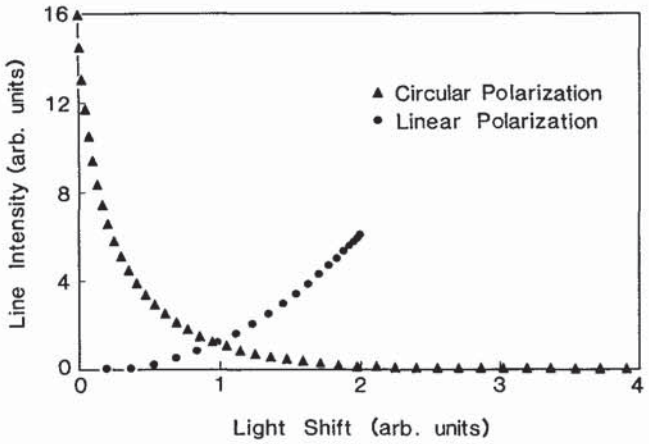

FIG. 5. Intensity of the (2 + 2) REMPI probability for each individual magnetic sublevel plotted as a function of the ac Stark shift in the case of the nondegenerate quadratic ac Stark effect [$O(20)$ line].

function of the light shift of each magnetic sublevel for excitation with linear and circular polarization, in the case of the quadratic ac Stark effect. The contrast is striking.

2. Spatial variation of the laser power density

To carry out efficient nonresonant multiphoton absorption, high laser power densities are required. The laser beam is therefore strongly focused, which means that the transverse and longitudinal variations of the laser power density in the probe volume must be taken into account. Each molecule encounters a different laser power density and accordingly undergoes a different light shift. The temporal structure of the pulse has not been characterized and is not taken into account; consequently, we assume a constant laser power. The signal $S(\omega)$ at ω is therefore obtained by integrating over the probe volume the line profile of each individual molecule

$$S(\omega)=\sum_M \int\int\int_V n(\mathbf{r})A(\mathbf{r})\Gamma_g(J,M,\mathbf{r})|\langle e|\psi_M(\mathbf{r})\rangle|^2 \times g[2\omega-\omega_M(\mathbf{r})]d^3r, \quad (28)$$

where $n(\mathbf{r})$ is the density of molecules at the point $\mathbf{r}$, $A(\mathbf{r})$ is the detection efficiency of the ion (or of the fluorescence photon in case of a LIF experiment) at the point $\mathbf{r}$, $g[2\omega-\omega_M(\mathbf{r})]$ includes all the line broadening effects other than the ac Stark effect (Doppler profile, laser bandwidth, natural linewidth, etc.) and $\omega_M(\mathbf{r})$ is the shifted resonance angular frequency of the level M for a power density $P(\mathbf{r})$, and $|\psi_M(\mathbf{r})\rangle$ is the corresponding wave function. The two-photon transition probability $\Gamma_g(J,M,\mathbf{r})$ depends on $\mathbf{r}$ only through $P(\mathbf{r})$, the radially dependent power density [see Eq. (25)]. The photoionization probability of the N_2 $a\,{}^1\Pi_g$ state is assumed to be constant and has therefore not been included. Thus, this treatment neglects possible broadening of the dressed state caused by one-photon coupling of the N_2 $o_3\,{}^1\Pi_u$ component with the continuum, a broadening mechanism that can be significant under some circumstances.[18]

It is convenient to study the influence of the ac Stark effect on the line profile independently of the other sources of broadening. This can be done using the relation

$$g[2\omega-\omega_M(\mathbf{r})]=\int_{-\infty}^{+\infty} g(2\omega-2\omega')\times\delta[2\omega'-\omega_M(\mathbf{r})]d(2\omega'), \quad (29)$$

which allows Eq. (28) to be rewritten as

$$S(\omega)=\int_{-\infty}^{+\infty} S_{ls}(\omega')g(2\omega-2\omega')d(2\omega'). \quad (30)$$

Here $S_{ls}(\omega')$ is the line profile arising only from the contribution of the ac Stark effect

$$S_{ls}(\omega)=\sum_M \int\int\int_V n(\mathbf{r})A(\mathbf{r})\Gamma_g(J,M,\mathbf{r})|\langle e|\psi_M(\mathbf{r})\rangle|^2 \times\delta[2\omega-\omega_M(\mathbf{r})]d^3r. \quad (31)$$

The detailed calculation of this integral is presented in the Appendix.

The profile of a single Zeeman component [see Eq. (A8)] for different values of the observation length z_1, is presented in Fig. 6 for the nondegenerate case. The relative power density $X_\pm = P_\pm/P_0$ varies approximately linearly with the frequency detuning. When the observation length z_1 is shorter than or comparable to the Rayleigh length z_R, the line profile is a triangle.[17,47] When the observation length is much longer than the Rayleigh length, then the weight of the less shifted points, corresponding to lower laser power, is increased.

The parameters used in the simulation of the spectra are listed in Table III. The laser beam parameters have been calculated from the optical system assuming a Gaussian beam. The laser bandwidth has been determined from unperturbed lines (low-J lines of the O branch); this includes also a small contribution from Doppler broadening. The transition dipole matrix element has been adjusted in order to reproduce the magnitude of the observed ac Stark effect. The contribution of the P, Q, and R-branch lines of the N_2 o_3–a transition have been included.

Figure 7 presents the line profile of the $O(10)$ to $O(23)$ lines in linear polarization [Fig. 7(a)] and circular polariza-

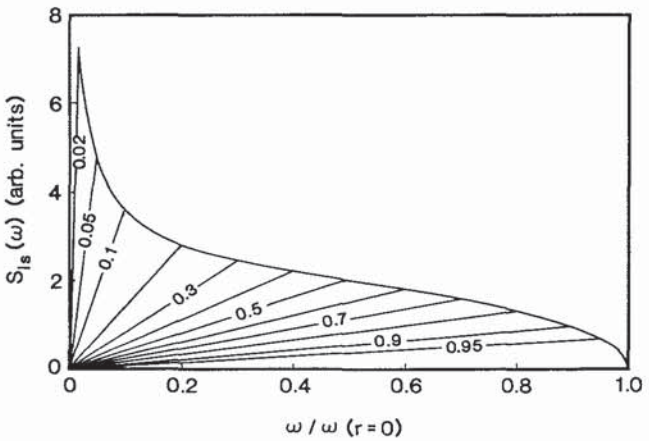

FIG. 6. Line profile of a single Zeeman component for different values of $z_R^2/(z_1^2+z_R^2)$.

TABLE III. Parameters used for the simulation of the ac Stark effect of the $a\ ^1\Pi_g$ state of N_2.

Parameter	Value
$\lvert\langle a\ ^1\Pi_g, v=1 \rVert d \rVert o_3\ ^1\Pi_u, v=0\rangle\rvert$	1.0×10^{-3} D
Laser bandwidth (FWHM)	0.08 cm^{-1}
Pulse energy	15 mJ
Estimated power density	1.2×10^{11} W/cm^2
Laser Rayleigh length, z_R	2.5 mm
Detection length, z_l	20 mm

tion [Fig. 7(b)]. The resonance at the $O(20)$ line stands out. In linear polarization, the asymmetric broadening increases progressively from $O(10)$ to $O(19)$. On this scale, the $O(20)$ line appears completely "flat." The broadening decreases from $O(21)$ to $O(23)$, and the asymmetry has an opposite sign. In circular polarization, only the $O(20)$ line is significantly affected by the ac Stark effect.

Figure 8 presents the experimental and theoretical widths of the O-branch lines in linear polarization. The agreement is excellent. Below the resonance (for $J\leqslant19$), the P, Q, and R-branch lines add their contribution to produce a light shift with the same sign. The linewidth increase is therefore smooth and progressive. On the other side of the resonance, R-branch lines on one hand, and P and Q-branch lines on the other hand produce shifts of opposite signs. The linewidths therefore drop more sharply. The experimental error bar of the $O(23)$ line is important to recall because this is the weakest line observed; this explains the discrepancy observed. For the lowest observed levels [namely $O(10)$], the relative contribution of the P-branch lines to the ac Stark effect is $\sim30\%$.

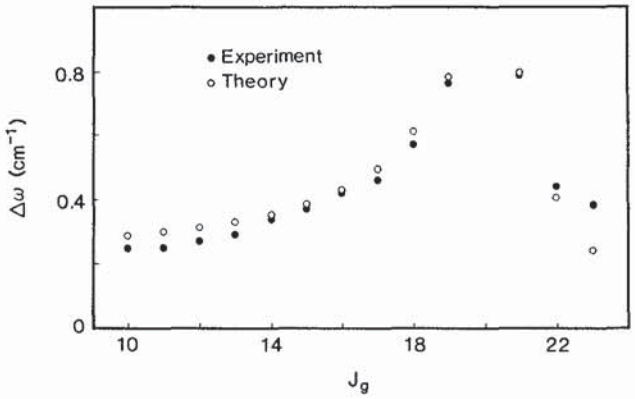

FIG. 8. Comparison of the experimental and theoretical linewidths for the $O(10)$ to $O(23)$ lines [the $O(20)$ line has been omitted].

Figure 9 presents a direct comparison of the polarization effect for the $O(20)$ line under excitation. The contrast is marked. In linear polarization, the spectrum appears as two humps, which is what is observed experimentally. The ac Stark effect is linear here (matrix elements of the coupling Hamiltonian larger than the energy separation), and the two resonances corresponding to $|\psi_+\rangle$ and $|\psi_-\rangle$ [see Eq. (14)] carry half of the total intensity; this is the Autler–Townes effect. The width of the features is caused by the superposition of the M sublevels, which have different splittings. In circular polarization, the $O(20)$ line is barely broadened and exhibits a small shoulder at the position corresponding to the three-photon resonance with the N_2 o_3–X transition. In this polarization, the magnetic sublevels with M close to $-J$ carry the strongest intensity, but the matrix

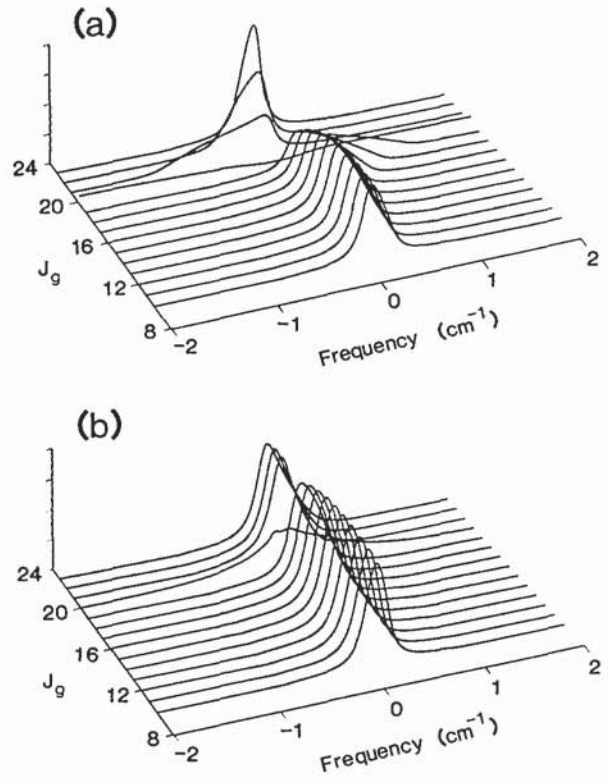

FIG. 7. Calculated line profiles of the $O(10)$ to $O(23)$ lines (a) linear polarization and (b) circular polarization. The $O(20)$ width is much larger than the frequency interval presented here.

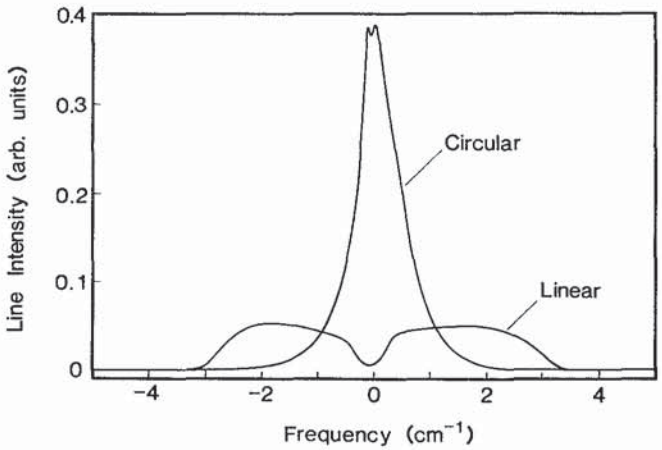

FIG. 9. Profile of the $O(20)$ line for linear and circular polarization.

elements of the coupling Hamiltonian are the smallest; in particular, they are smaller than the energy difference between the unperturbed levels [$|H_{ie,\pm}| \lesssim \hbar(\omega_{ie} - \omega)$]; the ac Stark effect is quadratic and the two-photon resonance carries most of the intensity. When M increases from $-J$ to $+J$, $|H_{ie,\pm}|$ increases and the ac Stark effect changes progressively from a quadratic to a linear dependence on the electric field strength. In this last case, the intensity of the transition is split between the two resonances, but it is also very small; the expected two humps do not appear.

In summary, the agreement between the experimental results and the theoretical simulations is excellent for the (2 + 2) REMPI detection of N_2, both qualitatively and quantitatively. Similar results are obtained on the P branch, but the resonance occurs between the $P(21)$ and the $P(22)$ lines, which explains why no line splitting was observed in this branch. The contrast between linear and circular polarization is less striking, as can be expected from the Hönl–London factors listed in Table I. These results give a good estimate of the transition dipole matrix element of the $N_2\, o_3$–a (0,1) band, even though the number of magnetic sublevels is important [when compared to the experiment performed on the ($v = 6, J = 1$) level of H_2 $E,F\,^1\Sigma_g^+$, for instance[26]], and also despite the characteristics of the laser beam, which are far from ideal as well as somewhat uncontrolled.

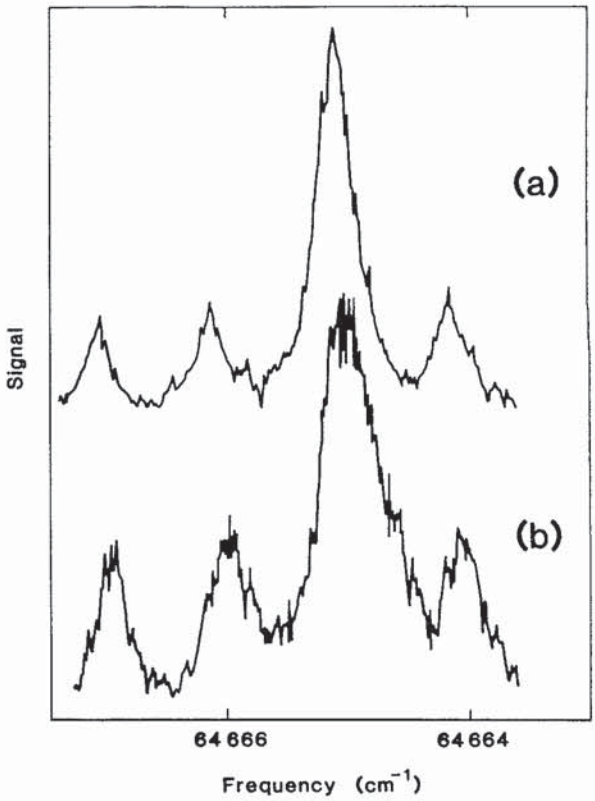

FIG. 10. Two-photon excitation spectrum of the CO $A\,^1\Pi, v' = 0$–$X\,^1\Sigma^+, v = 0$, $P(11)$ line (a) at low light intensity ($E = 320$ μJ; $P/S = 2.5\times10^9$ W/cm^2); (b) at high light intensity ($E = 1.7$ mJ; $P/S = 1.4\times10^{10}$ W/cm^2).

V. TWO-PHOTON LASER-INDUCED FLUORESCENCE OF CO

The ac Stark effect has been observed in the two-photon LIF of the CO $A\,^1\Pi$ state.[17,47] A near-UV laser beam is used to excite the CO $A\,^1\Pi$–$X\,^1\Sigma^+$ (0,0) band. The resonances are detected by collecting the vacuum-UV fluorescence. Asymmetrical line broadenings appear in the excitation spectra, taken with linearly polarized laser light. The linewidths exhibit a linear dependence on the power of the laser beam. These broadenings are produced by the nondegenerate ac Stark effect. We review here the experimental results, giving special emphasis to the geometry of the fluorescence detection system.

A. Experimental data

1. Apparatus

The experimental setup has already been described elsewhere.[17,47] Briefly, a linearly polarized excitation light beam ($\lambda \simeq 309$ nm, 2 mJ/pulse) is obtained by frequency doubling a Nd:YAG-pumped dye laser. The UV beam linewidth is ~ 0.08 cm^{-1}. The beam is focused into a CO cell by a fused-silica lens (focal length of 200 or 46 mm). The laser power is varied by placing a set of fused-silica plates in the beam path, which does not affect the laser linewidth.

The CO $A\,^1\Pi$–$X\,^1\Sigma^+$ fluorescence is detected by a solar-blind photomultiplier, which views the molecular sample along the direction of linear polarization of the incident light beam. The laser wavelength is tuned by tilting the intracavity Fabry–Pérot interferometer (Littrow-type cavity).[53] The wavelength calibration is obtained by comparison with the iodine fluorescence spectrum (excited with visible light).[54]

2. Results and qualitative discussion

Figure 10 presents the fluorescence spectrum of the $P(11)$ line of the (0,0) band recorded at two different laser powers (320 μJ/pulse and 1.7 mJ/pulse). At high power densities, the line is shifted, broadened, and becomes asymmetric. Figure 11 presents the variation of the linewidth with laser power and compares this to the result of the theoretical simulation. Particularly pronounced is the linear variation of the linewidth with laser power, which is expected from Eq. (9), as soon as the linewidth exceeds the laser linewidth and Doppler broadening contribution to the width.

Data on other rotational levels are limited. No splitting appears, as was observed in the case of N_2. This means that the identification of the state producing the ac Stark effect is less straightforward than in the case of N_2, and that the shift results most probably from the contribution of several states. Lying below the $A\,^1\Pi$ state are triplet states.[55] Of these, the lowest one, the $a\,^3\Pi$ state, lies 16 400 cm^{-1} below the A state, whereas the photon energy is 32 400 cm^{-1}; thus, their contribution is negligible. Above the A state, the $B\,^1\Sigma^+$, $C\,^1\Sigma^+$, and $E\,^1\Pi$ Rydberg states have vibrational levels that are < 1000 cm^{-1} away from resonance. Moreover, these states have reasonably strong transition dipole moment matrix elements connecting them to the A state.[56]

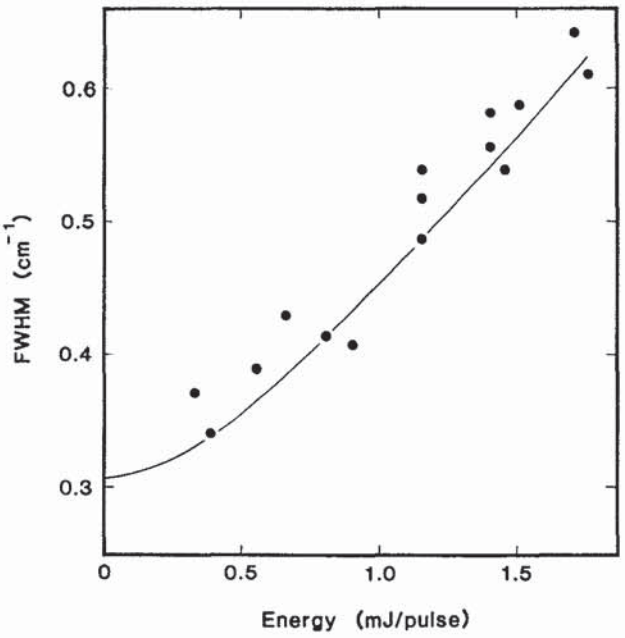

FIG. 11. Variation of the full-width at half-maximum of the $P(11)$ line as a function of the laser energy. Here the solid circles represent experimental measurements and the solid curve is theory. [Calculated with the following data: laser bandwidth (HWHM) = 0.036 cm^{-1}, Doppler width (HWHM) = 0.069 cm^{-1}.]

B. Simulation of observed line profiles

1. Intensity of individual magnetic sublevels

Because the CO $A\,^1\Pi$–$X\,^1\Sigma^+$ two-photon transition has no resonant intermediate level,[55] the excitation of the A state is in the nonsaturated regime. Its probability is therefore given by the two-photon line strength[44–47] [see Eq. (25)]. The fluorescence signal does not depend solely on the excitation process but also on the detection efficiency; each magnetic sublevel $|J',M'\rangle$ radiates with a given geometrical pattern (which depends on M' and on the parallel or perpendicular character of the transition); its detection efficiency depends therefore on the direction of observation, i.e., on the direction of the photomultiplier tube (PMT) with respect to the linear polarization of the incident light beam.

The calculation can be carried out in a manner similar to Eq. (25) for the M-dependent one-photon fluorescence by summing the transition probabilities corresponding to the two directions of polarization that can be detected (in the absence of a polarization analyzer in the detection channel). However, a more convenient way to treat this optical pumping cycle is to use the density matrix formalism.[57] Even in this simple case, in which the evolution of excited-state populations is given by the diagonal part of the density matrix, this formalism allows us to derive a simple expression for the line intensity using irreducible tensorial operators.

The fluorescence intensity of one magnetic sublevel $|e',J',M'\rangle$ is given by[57–61]

$$I_{M'} = \left(\frac{P}{Sc}\right)^2 \frac{3}{2\pi\hbar^2\epsilon_0^2\Delta\omega_L}\langle e',J',M'|\mathscr{E}\cdot\mathscr{D}|e',J',M'\rangle, \tag{32}$$

where $\mathscr{E}$ is the operator describing the density matrix of the excited state $|e',J',M'\rangle$ arising from the two-photon excitation process

$$\mathscr{E} = \sum_M Q\,|f,J,M\rangle\langle f,J,M|\,Q^* \tag{33}$$

and $\mathscr{D}$ is the operator associated with the detection probability of an excited state $|e',J',M'\rangle$ by a fluorescent transition to all the possible levels $|f'',J'',M''\rangle$,

$$\mathscr{D} = \sum_{f'',J'',M''} \mathbf{D}\cdot\boldsymbol{\epsilon}'|f'',J'',M''\rangle\langle f'',J'',M''|(\mathbf{D}\cdot\boldsymbol{\epsilon}')^*, \tag{34}$$

where $\boldsymbol{\epsilon}'$ is the polarization of the detected light.

In the case of REMPI, we have assumed a detectivity operator $\mathscr{D}$ independent of J' and M'. The line intensity is in this case directly proportional to the matrix element of $\mathscr{E}$, which has been given in Eq. (25). We detail now the calculation of the matrix elements of $\mathscr{E}$ and of $\mathscr{D}$ in the case of fluorescence detection.

In Eq. (33), Q is the two-photon absorption operator, which has an expression similar to the light shift operators $\Delta_\pm$ defined by Eq. (10) [$\Delta_+ + \Delta_-$ is the diagonal part of a generalized operator describing the (one-color) two-photon processes; Q is the nondiagonal part],

$$Q = \sum_i \mathbf{D}\cdot\boldsymbol{\epsilon}\,\frac{|i\rangle\langle i|}{\hbar(\omega-\omega_{if})}\,\mathbf{D}\cdot\boldsymbol{\epsilon}. \tag{35}$$

Using the same approximation as for the light shift operator, the two-photon absorption operator can be expressed [see Eq. (21)] as

$$Q = \sum_{K,Q,N} a_Q^{(K)} q_N^{(K)} D^{(K)}_{Q,N}(\phi,\theta,\chi), \tag{36}$$

where expressions for $a_Q^{(K)}$ and $q_N^{(K)}$ have been given in Eqs. (26) and (27). The operator Q results from the combination of two operators of rank 1; its rank is therefore $\leqslant 2$. Moreover, Q is a symmetrical operator. Consequently, its decomposition is limited to symmetrical operators so that K can only have the values 0 or 2. Hence, the matrix elements of $\mathscr{E}$ are given by

$$\begin{aligned}&\langle e',J',M'|\mathscr{E}|e',J',M'_1\rangle \\ &= \sum_{k,k',q,q',n,n'} a_q^{(k)} a_{q'}^{(k')*}\langle e'|q_n^{(k)}|f\rangle\langle e'|q_{n'}^{(k')}|f\rangle^* \\ &\quad\times(-1)^{M'-M'_1}\sum_{M,\Omega}\begin{pmatrix} J' & k & J\\ -M' & q & M\end{pmatrix}\begin{pmatrix} J' & k' & J\\ -M'_1 & q' & M\end{pmatrix}\begin{pmatrix} J' & k & J\\ -\Omega' & n & \Omega\end{pmatrix}\begin{pmatrix} J' & k' & J\\ -\Omega' & n & \Omega\end{pmatrix}.\end{aligned} \tag{37}$$

In the CO $A\,^1\Pi$–$X\,^1\Sigma^+$ transition, $|\Delta\Omega| = 1$ and the $k = 0$ term vanishes in Eq. (37). The summation is therefore limited to the terms $k = k' = 2$. As the polarization of the laser is linear, the only nonvanishing term is $a_0^{(2)}$, which means that $q = q' = 0$. Hence, Eq. (37) reduces to one term,

$$\langle e',J',M'|\mathscr{E}|e',J',M_1'\rangle = \delta_{M',M_1'}|a_0^{(2)}|^2|\langle e'|q_n^{(2)}|f\rangle|^2 \times \begin{pmatrix} J' & 2 & J \\ -1 & 1 & 0 \end{pmatrix}^2 \begin{pmatrix} J' & 2 & J \\ -M' & 0 & M_1' \end{pmatrix}^2. \tag{38}$$

The decomposition of $\mathscr{D} = \Sigma_{K,Q}\mathscr{D}_Q^{(K)}T_Q^{(K)}$ in terms of the irreducible tensor operators $T_Q^{(K)}$ defined by[36,62]

$$T_Q^{(K)} = \sum_{M,M'} (-1)^{K+Q+J+M}[2K+1]^{1/2} \times \begin{pmatrix} J & J & K \\ -M' & M & Q \end{pmatrix}|JM'\rangle\langle JM|, \tag{39}$$

is well known.[58] The detection of a photon having a polarization direction ϵ' is given by

$$\mathscr{D}_Q^{(K)}(\epsilon') = \sum_{J'',f''}\left[\sum_{p,p'}\epsilon'_{-p}(\epsilon'^*)_{-p'}\begin{pmatrix} 1 & 1 & K \\ -p & -p' & Q \end{pmatrix}\right] \times|\langle e'\|d^{(1)}\|f''\rangle|^2(2J'+1) \times(2J''+1)\begin{pmatrix} J' & 1 & J'' \\ -\Omega' & n & \Omega'' \end{pmatrix}^2(-1)^{J''+J'} \times[2K+1]^{1/2}\begin{Bmatrix} 1 & 1 & K \\ J' & J' & J'' \end{Bmatrix}. \tag{40}$$

The summation over J'' and f'' corresponds to the nonselectivity of the detection process (f'' can represent, for instance, the different vibrational levels) and $\langle e'\|d^{(1)}\|f''\rangle = \mu_{e'f''}$ is the reduced matrix element (independent of J') of the electric dipole transition.

We apply this result to our particular geometry (see Fig. 12), in which excitation laser polarization is along the Z direction, which is also the direction of detection (and the quantization axis). The detector (a photomultiplier tube) does not select any particular polarization. This means that the contributions of both ϵ_x and ϵ_y polarizations must be added incoherently or, in an equivalent way, the contributions of both circular polarizations ϵ_+ and ϵ_-. The electronic transition is a Π–Σ^+ transition. The upper state has two components $\Pi(A')$ and $\Pi(A'')$ (according to the new convention[63]) of parity $(-1)^J$ and $(-1)^{J+1}$, respectively, while the $X\,^1\Sigma^+$ ground state has only one component with parity $(-1)^J$. Accordingly, the $\Pi(A')$ component can be excited by the O, Q, and S two-photon transitions and reradiate by the one-photon spontaneous emission P and R transition lines. Similarly, the $\Pi(A'')$ component is excited by P and R two-photon lines and reradiates only Q lines. Hence, the matrix elements of $\mathscr{D}$ are given for these two different cases by

$$\langle J',M',\Pi(A')|\mathscr{D}|J',M',\Pi(A')\rangle = \mu_{e'f''}^2\left[\frac{2J'^2+2J'-3}{(2J'-1)(2J'+3)} + \frac{M'^2(2J'^2+2J'+3)}{J'(J'+1)(2J'-1)(2J'+3)}\right] \tag{41a}$$

and

$$\langle J',M',\Pi(A'')|\mathscr{D}|J',M',\Pi(A'')\rangle = \mu_{e'f''}^2\frac{J'(J'+1)-M'^2}{J'(J'+1)}. \tag{41b}$$

Because $\mathscr{E}$ has only diagonal elements, we have limited our calculation to the diagonal elements of $\mathscr{D}$.

These equations have been used to calculate the profile of the $P(11)$ line. The variation of the power density along the laser profile has been taken into account exactly in the same way as for the REMPI of N_2 (see above and Appendix).

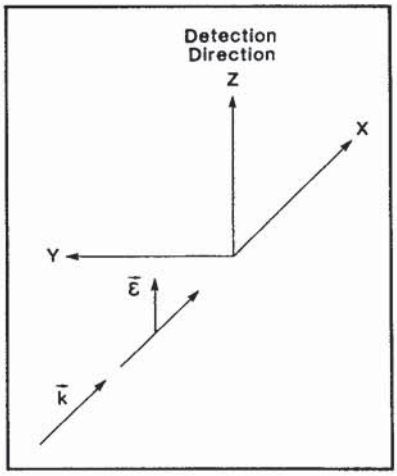

FIG. 12. Geometry of the experiment. The laser ($\mathbf{k}$ vector) is directed along the X axis and is polarized (ϵ) along the Z axis. The photomultiplier detects photons emitted in the Z direction.

2. Quantitative evaluation of the light shift

The CO $A\,^1\Pi$ state is described by Hund's coupling case (a). It is a linear combination of the $|\Omega = +1\rangle$ and $|\Omega = -1\rangle$ components. The ac Stark shift is therefore given by

$$\Delta E = \frac{P}{2\epsilon_0 cS}[A(1,1) \pm A(1,-1)], \tag{42}$$

where $A(1,-1)$ is nonvanishing only if there are contributions from $\Omega_i = 0$ states ($^1\Sigma^+$ or $^1\Sigma^-$ states in this case) and the $+$ and $-$ signs correspond to the A' and A'' components, respectively. This total shift can be split into four terms corresponding to the different possible values of the perturbing state Ω_i (0^+, 0^-, 1, or 2),

$$\Delta E = \Delta E_{0^+} + \Delta E_{0^-} + \Delta E_1 + \Delta E_2. \tag{43}$$

Each of these terms has a specific angular dependence (which depends only on the value of Ω_i) and a specific amplitude, which depends on the detailed characteristics of the intermediate states (energy, transition dipole moment), $\Delta E_\Omega = (P/2\epsilon_0 cS)F_\Omega(M,J)S_\Omega$. Most of this information is

TABLE IV. Angular dependence of the contribution of the $\Omega_i = 0^+, 0^-$, 1, and 2 intermediate states to the ac Stark effect of the $\Pi(A'')$ component. For the $\Pi(A')$ component, the contributions of the 0^+ and 0^- intermediate states are exchanged.

$F_{\Omega_i}(M,J)$	Expression
$F_{0^-}(M,J)$	$\dfrac{M^2}{J(J+1)}$
$F_{0^+}(M,J)$	$\dfrac{2J^2(J+1)^2 - M^2(2J^2+2J+3)}{J(J+1)(2J+3)(2J-1)}$
$F_1(M,J)$	$\dfrac{J(J+1)(2J^2+2J-3) - 2M^2(J^2+J-3)}{J(J+1)(2J+3)(2J-1)}$
$F_2(M,J)$	$\dfrac{J^2(J+1)^2 - M^2(J^2+J-3)}{J(J+1)(2J+3)(2J-1)}$

lacking as some of these intermediate states lie above the dissociation limit and have not been observed (or the transition connecting to the $A\ ^1\Pi$ state has not been observed). It is therefore not possible to calculate either the total magnitude of ΔE or its total angular dependance.

We shall only give here the angular dependence of these four terms (see Table IV) and calculate the magnitude of ΔE_{0^-} for which the largest amount of information is available. The detail of the contribution of several vibrational levels of the $X\ ^1\Sigma^+$, $B\ ^1\Sigma^+$, and $C\ ^1\Sigma^+$ states is given in Table V. Only the first few vibrational levels of the B and C states have been observed. For these states, we give two values, the first resulting from taking into account only the observed levels and the second by including higher vibrational levels (whose positions have been extrapolated from the lowest levels). For these levels, the Franck–Condon factors of the $(B$–$A)$ and $(C$–$A)$ transitions have been borrowed from the $(A$–$X)$ transition[56] as the X, B, and C states are nearly parallel. The contribution of the unobserved levels is predominant but uncertain, the $(B\ ^1\Sigma^+, v'=5)$ alone accounting for 70% of the total. For this level, the energy defect is only 30 cm^{-1} and is affected by a large error bar. The experimental value has a sign opposite to the one of these various calculated values, but an increase of the position of the $B\ ^1\Sigma^+, v'=5$ level by 100 cm^{-1} would be enough to account for the experimental value. Higher lying Rydberg states and their continua, for which little is known, would also contribute to a negative shift. In spite of limited information on the states involved, it is remarkable that this calculation can indicate the order of magnitude of this effect.

TABLE V. Detailed contribution of the X, B, and C states to the ac Stark effect (S_{0^-}) of the $A\ ^1\Pi(A'')$, $v'=0$, $J'=10$ level [excited by the $P(11)$ two-photon line at a laser frequency of 32 330 cm^{-1}]; units are D^2/cm^{-1}. (a) Only observed vibrational levels are taken into account; (b) contributions from unobserved vibrational levels are included.

	$X\ ^1\Sigma^+$	$B\ ^1\Sigma^+$	$C\ ^1\Sigma^+$	Total
S_{0^-} (a)	6.8×10^{-5}	2.9×10^{-4}	3.2×10^{-4}	6.8×10^{-4}
S_{0^-} (b)	6.8×10^{-5}	4.1×10^{-3}	7.6×10^{-4}	4.9×10^{-3}
S_{0^-} (expt)				-1.5×10^{-3}

VI. CONCLUDING REMARKS

We have presented a detailed analysis of the ac Stark effect for a diatomic molecule. A thorough understanding of this effect is necessary in carrying out REMPI experiments because quasiresonances with high-lying Rydberg states are highly probable, given the high density of such states. Moreover, with the high laser intensity commonly used, Rabi oscillations may be large (up to hundreds of wave numbers).

In the ac Stark effect observed in both experimental cases presented here, only the excited state is significantly shifted. The shift of the ground state is negligible because this state is far from resonance (the first resonance occurs after absorption of two photons). More generally, the ac Stark effect of a ground state may be significant. The ac Stark effect can then be considered as equivalent to the application of an external field, which can be used to manipulate molecules as it is used for atoms. One possibility is the laser cooling of molecules. In such a process the velocity change of the emitter caused by spontaneous emission occurs in a random direction, whereas the absorption occurs in the direction of the laser beam. For each cycle of absorption followed by spontaneous emission the momentum of the emitter is reduced only by a quantity lying between 0 and $2\hbar k$. Hence a large number of cycles are required, and the emitter must remain in resonance, i.e., act essentially as a two-level system. Few molecules appear to satisfy these criteria. Another application of the ac Stark effect to manipulate molecular systems may be to focus or defocus molecules in a selected state in a molecular beam. This task appears to be less demanding than laser cooling.

ACKNOWLEDGMENTS

We thank Andrew C. Kummel for his help in the N_2 $(2+2)$ REMPI experiment and Katharine L. Reid and David J. Leahy for fruitful discussions. B. G. thanks NATO and CNRS for postdoctoral fellowship support. This work is supported by the Office of Naval Research under Contract No. N00014-91-J-1023.

APPENDIX: DETAILED CALCULATION OF THE LINE PROFILE

The ac Stark effect line profile is given by Eq. (31),

$$S_{ls}(\omega) = \sum_M \int\int\int n(\mathbf{r})A(\mathbf{r})\Gamma_g(J,M,\mathbf{r})|\langle e|\psi_M(\mathbf{r})\rangle|^2 \times\delta[2\omega - \omega_M(\mathbf{r})]d^3\mathbf{r}, \quad \text{(A1)}$$

where the quantities in the integrand have already been defined. We assume here the transverse variations of the detection efficiency $A(\mathbf{r})$ to be negligible compared to the laser beam waist and that the longitudinal variation can be modeled by a square function,

$$A(z) = \begin{cases} A_0 & \text{for } -z_1 \leqslant z \leqslant z_1 \\ 0 & \text{otherwise} \end{cases}.$$

We also take $\Gamma_g(J,M,\mathbf{r}) = P^2(\mathbf{r})I(J,M)$ as the photoionization (or excitation) probability, where $P(\mathbf{r})$ is the radiation density at the distance $\mathbf{r}$ measured from the center of the beam line and $I(J,M)$ represents the remaining factors in Eq. (25). In Eq. (A1) $\langle e|\psi_M(\mathbf{r})\rangle$ and $\omega_M(\mathbf{r})$ are obtained by diagonalizing the total Hamiltonian of the system H [see Eq. (4)] for a given laser power $P(\mathbf{r})$ (the frequency origin is taken at the ground state). To derive an analytic expression of the line profile, we assume that at most one level $|i\rangle$ is close to resonance. The contribution of this level $|i\rangle$ is evaluated through an exact diagonalization, and the contribution of all other levels $|i'\rangle$ is calculated using second-order perturbation theory,

$$\omega_{M\pm}(\mathbf{r}) = \frac{\omega_e + \omega_i - \omega}{2} \pm \tfrac{1}{2}[\Delta\omega^2 + 4\alpha_M P(\mathbf{r})]^{1/2} - \sum_{i'} \alpha'_M P(\mathbf{r}) \frac{2\omega_{i'e}}{(\omega_{i'e}^2 - \omega^2)}, \tag{A2}$$

where $\Delta\omega = \omega_{ie} - \omega$ and

$$|\langle e|\psi_{M\pm}(\mathbf{r})\rangle|^2 = \frac{2\alpha_M P(\mathbf{r})}{\Delta\omega^2 + 4\alpha_m P(\mathbf{r}) \pm \Delta\omega[\Delta\omega^2 + 4\alpha_m P(\mathbf{r})]^{1/2}}, \tag{A3}$$

with the shorthand notation $|H_{ie,\pm}|^2 = \alpha_M P(\mathbf{r})\hbar^2$ and $|H_{i'e,\pm}|^2 = \alpha'_M P(\mathbf{r})\hbar^2$. We have neglected the contribution of the other levels $|i'\rangle$ to the projection of the wave function on the level $|e\rangle$ as this contribution is much smaller than unity.

We assume that the laser beam has a Gaussian profile

$$P(r,z) = P_0 \frac{1}{w(z)^2} \exp\left[-\frac{2r^2}{w(z)^2}\right], \tag{A4}$$

where P_0 is the maximum laser power (at the focus) and $w(z)$ is the beam waist (half-width at $1/e$ height) at a distance z from the focus, given by

$$w(z) = w_0^2 \frac{z^2 + z_R^2}{z_R^2}, \tag{A5}$$

where z_R is the Rayleigh length and w_0 is the beam waist at the focus.

Equation (A1) can be rewritten as

$$S_{ls}(\omega) = 2\pi nA \sum_M \int_{-z_1}^{z_1} dz \int_0^\infty rdrI(J,M)P^2(\mathbf{r}) \times |\langle e|\psi_M(\mathbf{r})\rangle|^2 \delta[2\omega - \omega_M(\mathbf{r})]. \tag{A6}$$

The integration over r requires finding the zeros of the delta function. These are the zeros, which we call $P_\pm = X_\pm P_0$ of the second-degree equation

$$4\left[\sum_{i'} \frac{\alpha'_M \omega_{i'e}}{(\omega_{i'e}^2 - \omega^2)}\right]^2 P(\mathbf{r})^2 - \left[\alpha_M + (\omega_e + \omega_i - S_\omega) \times \sum_{i'} \frac{\alpha'_M \omega_{i'e}}{(\omega_{i'e}^2 - \omega^2)}\right] P(\mathbf{r}) + (\omega_i - 3\omega)(\omega_e - 2\omega) = 0. \tag{A7}$$

The only physically acceptable solutions are those for which $0 \leqslant X_\pm \leqslant 1$. At a distance z from the focus, the maximum power is $P(0,z) = P_0[z_R^2/(z^2 + z_R^2)]$, which limits the accessible range to $0 \leqslant X_\pm \leqslant [z_R^2/(z^2 + z_R^2)]$. On the other hand, at a given angular frequency ω, the range of longitudinal positions that contribute to the signal is limited to $|z| \leqslant \min(z_+, z_1)$ with $z_\pm = z_R[(1 - X_\pm)/X_\pm]^{1/2}$. The integration over r of Eq. (A6) therefore yields

$$S_{ls}(\omega) = \pi nA_0 \sum_M I(J,M) \sum_{k=+,-} \frac{P_k |\langle e|\psi_M(P_k)\rangle|^2}{\left|\left(\frac{d\omega_M}{dP}\right)_{P=P_k}\right|} \int_0^{\min(z_k,z_1)} \omega(z)^2 dz$$

$$= \frac{\pi}{3} nA_0 P_0 \sum_M I(J,M) \sum_{k=+,-} \frac{|\langle e|\psi_M(P_k)|\rangle|^2}{\left|\left(\frac{d\omega_M}{dP}\right)_{P=P_k}\right|} \times z_r \begin{cases} \frac{X_k}{X_1}(1 + 2X_1)[(1 - X_1)/(X_1 - 1)]^{1/2} & \text{for } z_1 \leqslant z_k \\ (1 + 2X_k)[(1 - X_k)/X_k]^{1/2} & \text{for } z_1 \geqslant z_k \end{cases}, \tag{A8}$$

where

$$\left(\frac{d\omega_M}{dP}\right)_{P=P_k} = \alpha_M \Big/ \left[5\omega - (\omega_e + \omega_i) + \sum_{i'} \alpha'_M P_k \frac{2\omega_{i'e}}{\omega_{i'e}^2 - \omega^2}\right] - \sum_{i'} \alpha'_M \frac{2\omega_{i'e}}{\omega_{i'e}^2 - \omega^2}. \tag{A9}$$

[1] H. Lefebvre-Brion and R. W. Field, *Perturbations in the Spectra of Diatomic Molecules* (Academic, New York, 1986).
[2] G. O. Sitz, Ph.D. thesis, Stanford University, 1987.
[3] S. H. Autler and C. H. Townes, Phys. Rev. **100**, 703 (1955).
[4] C. Cohen-Tannoudji, Ann. Phys. (Paris) **7**, 423 (1962); **7**, 469 (1962); A. M. Bonch-Bruevich and V. A. Khodovoi, Usp. Fiz. Nauk **93**, 71 (1967) [Sov. Phys. Usp. **10**, 637 (1968)].
[5] (a) S. Feneuille, Rep. Prog. Phys. **40**, 1257 (1977); (b) P. L. Knight and P. W. Milonni, Phys. Rep. **66**, 21 (1980).
[6] M. D. Levenson and S. S. Kano, *Introduction to Nonlinear Laser Spectroscopy* (Academic, New York, 1988).
[7] E. B. Aleksandrov, A. M. Bonch-Bruevich, N. N. Kostin, and V. A. Khodovoi, Zh. Eksperim. i Teor. Fiz. Pis'ma v Redakstiyu **3**, 85 (1966) [Sov. Phys. JETP Lett. **3**, 53 (1966)].

[8] J. E. Bjorkholm and P. F. Liao, Opt. Commun. **21**, 132 (1977); S. E. Moody and M. Lambropoulos, Phys. Rev. A **15**, 1497 (1977); H. R. Gray and C. R. Stroud, Jr., Opt. Commun. **25**, 359 (1978).
[9] A. Schabert, R. Keil, and P. E. Toschek, Appl. Phys. **6**, 181 (1975); P. F. Liao and J. E. Bjorkholm, Phys. Rev. Lett. **34**, 1 (1975).
[10] A. Aspect *et al.*, Phys. Rev. Lett. **57**, 1688 (1986); J. Dalibard and C. Cohen-Tannoudji, J. Opt. Soc. Am. B **6**, 2023 (1989); P. J. Ungar *et al.*, *ibid.* **6**, 2058 (1989).
[11] M. Brune, S. Haroche, V. Lefevre, J. M. Raimond, and N. Zagury, Phys. Rev. Lett. **65**, 976 (1990).
[12] B. Cagnac, G. Grynberg, and F. Biraben, J. Phys. (Paris) **34**, 845 (1973).
[13] A. C. Kummel, G. O. Sitz, and R. N. Zare, J. Chem. Phys. **88**, 7357 (1988).
[14] C. E. Otis and P. M. Johnson, Chem. Phys. Lett. **83**, 73 (1981).
[15] L. Li, R. N. Porter, and P. M. Johnson, Phys. Rev. Lett. **53**, 1336 (1984).
[16] W. R. Garrett, W. R. Ferrell, J. C. Miller, and M. G. Payne, Phys. Rev. A **32**, 3790 (1985).
[17] B. Girard, N. Billy, J. Vigué, and J. C. Lehmann, Chem. Phys. Lett. **102**, 168 (1983).
[18] W. M. Huo, K. P. Gross, and R. L. McKenzie, Phys. Rev. Lett. **54**, 1012 (1985).
[19] H. Pummer, H. Egger, T. S. Luk, T. Srinivasan, and C. K. Rhodes, Phys. Rev. A **28**, 795 (1983).
[20] T. Srinivasan, H. Egger, T. S. Luk, H. Pummer, and C. K. Rhodes, IEEE J. Quantum Electron. **QE-19**, 1874 (1983).
[21] N. Bjerre, R. Kachru, and H. Helm, Phys. Rev. A **31**, 1206 (1985).
[22] D. W. Chandler and L. R. Thorne, J. Chem. Phys. **85**, 1733 (1986).
[23] S. Ganguly and K. Rai Dastidar, Phys. Rev. A **37**, 1363 (1988).
[24] C. Y. Tai, R. T. Deck, and C. Kim, Phys. Rev. A **37**, 163 (1988).
[25] H. Moosmüller, C. Y. She, and W. M. Huo, Phys. Rev. A **40**, 6983 (1989).
[26] M. A. Quesada, A. M. F. Lau, D. H. Parker, and D. W. Chandler, Phys. Rev. A **36**, 4107 (1987).
[27] B. Garraway, K. A. Suominen, and S. Stenholm, in *Light Induced Kinetic Effects on Atoms, Ions and Molecules*, edited by L. Moi, S. Gozzini, C. Gabbanini, E. Arimondo, and F. Strumia (ETS Editrice, Pisa, 1991); B. Garraway and S. Stenholm, Opt. Commun. **83**, 349 (1991).
[28] J. D. Jackson, *Classical Electrodynamics* (Wiley, New York, 1962).
[29] E. T. Jaynes and F. W. Cummings, Proc. IEEE **51**, 89 (1963); C. Cohen-Tannoudji and S. Haroche, J. Phys. (Paris) **30**, 125 (1969); **30**, 153 (1969).
[30] C. Cohen-Tannoudji, B. Diu, and F. Laloe, *Quantum Mechanics* (Hermann, Paris, 1977; Wiley, New York, 1977).
[31] G. Grynberg, B. Cagnac, and F. Biraben, in *Coherent Nonlinear Optics, Recent Advances*, edited by M. S. Feld and V. S. Letokhov (Springer, Berlin, 1980), p. 111.
[32] A. M. F. Lau, Springer Ser. Chem. Phys. (Laser Induced Processes Mol.) **6**, 167 (1979); Phys. Rev. Lett. **43**, 1009 (1979).
[33] J. M. Brown and B. J. Howard, Mol. Phys. **31**, 1517 (1976).
[34] J. T. Hougen, Natl. Bur. Stand. (U.S.) Monogr. 115 (1970).
[35] B. R. Judd, *Angular Momentum Theory for Diatomic Molecules* (Academic, New York, 1972).
[36] R. N. Zare, *Angular Momentum, Understanding Spatial Effects in Chemistry and Physics* (Wiley, New York, 1988).
[37] C. H. Greene and R. N. Zare, J. Chem. Phys. **78**, 6741 (1983).
[38] G. O. Sitz, A. C. Kummel, and R. N. Zare, J. Chem. Phys. **89**, 2558 (1988).
[39] G. O. Sitz, A. C. Kummel, R. N. Zare, and J. C. Tully, J. Chem. Phys. **89**, 2572 (1988).
[40] A. C. Kummel, G. O. Sitz, R. N. Zare, and J. C. Tully, J. Chem. Phys. **89**, 6947 (1988).
[41] A. C. Kummel, G. O. Sitz, R. N. Zare, and J. C. Tully, J. Chem. Phys. **91**, 5793 (1989).
[42] G. D. Kubiak, G. O. Sitz, and R. N. Zare, J. Chem. Phys. **83**, 2538 (1985).
[43] K. L. Carleton, S. R. Leone, and K. H. Welge, Chem. Phys. Lett. **115**, 492 (1985).
[44] R. G. Bray and R. M. Hochstrasser, Mol. Phys. **31**, 1199 (1976).
[45] K. Chen and E. S. Yeung, J. Chem. Phys. **69**, 43 (1978).
[46] J. B. Halpern, H. Zacharias, and R. Wallenstein, J. Mol. Spectrosc. **79**, 1 (1980).
[47] B. Girard, Thèse de 3ème cycle, Université Pierre et Marie Curie, Paris, 1983 (unpublished).
[48] P. K. Carroll and C. P. Collins, Can. J. Phys. **47**, 563 (1969).
[49] J. T. Vanderslice, S. G. Tilford, and P. G. Wilkinson, Astrophys. J. **141**, 395 (1964).
[50] A. Lofthus and P. H. Krupenie, J. Phys. Chem. Ref. Data **6**, 113 (1977).
[51] K. Yoshino, Y. Tanaka, P. K. Carroll, and P. Mitchell, J. Mol. Spectrosc. **54**, 87 (1975).
[52] P. K. Carroll, C. P. Collins, and K. Yoshino, J. Phys. B **3**, L127 (1970); K. Yoshino (private communication, 1990).
[53] T. W. Hänsch, Appl. Opt. **11**, 895 (1972).
[54] S. Gerstenkorn and P. Luc, *Atlas d'absorption de la molécule d'iode* (CNRS, Paris, 1978).
[55] K. P. Huber and G. Herzberg, *Molecular Spectra and Molecular Structure. IV. Constants of diatomic molecules* (Van Nostrand Reinhold, New York, 1979).
[56] T. A. Carlson, N. Durie, P. Erman, and M. Larsson, Z. Phys. A **287**, 123 (1978).
[57] J. P. Barrat and C. Cohen-Tannoudji, J. Phys. Radiat. **22**, 22 (1961); **22**, 443 (1961).
[58] W. Happer and E. B. Salomon, Phys. Rev. **23**, 160 (1967).
[59] G. Gouédard and J. C. Lehmann, J. Phys. (Paris) **34**, 693 (1973).
[60] M. Broyer, G. Gouédard, J. C. Lehmann, and J. Vigué, Adv. At. Mol. Phys. **12**, 165 (1976).
[61] A. Omont, *Progress in Quantum Electronics* (Pergamon, Oxford, 1977), Vol. 5, Part 2, p. 69.
[62] U. Fano, Rev. Mod. Phys. **29**, 74 (1957).
[63] M. H. Alexander *et al.*, J. Chem. Phys. **89**, 1749 (1988).